Am J Transl Res 2020;12(7):3822-3841
www.ajtr.org /ISSN:1943-8141/AJTR0107988

Original Article

Homocysteine-induced electrical remodeling via the mediation of IP_3R1/Nav1.5 signaling pathway

Lu Han, Aping Wu, Qing Li, Zhen Xia, Yanqing Wu, Kui Hong, Zirong Xia, Juxiang Li

Department of Cardiovascular Medicine, The Second Affiliated Hospital of Nanchang University, Nanchang 330006, China

Received January 16, 2020; Accepted June 3, 2020; Epub July 15, 2020; Published July 30, 2020

Abstract: Inositol-1,4,5-triphosphate-receptor 1 (IP_3R1), a Ca^{2+} channel in the sarcoplasmic reticulum membrane, is an effective regulator of Ca^{2+} release involved in the pathology of most cardiovascular diseases. Our study aim to investigate the underlying mechanism by which IP_3R1 signaling mediates the process of homocysteine (Hcy)-induced Ca^{2+} accumulation via interaction with sodium current (Nav1.5) in atrium. We utilized whole-cell patch-clamp analysis and flow cytometry to detect the abnormal electrical activity in mouse atrial myocytes (MACs) obtained from C57B6 mice fed with high-Hcy diet. The results represented not only an increase in protein levels of Nav1.5 and IP_3R1, but also an enhanced intracellular levels of Ca^{2+}, and prolonged action potential duration (APD). However, the inhibition of IP_3R1 or Nav1.5 gene could both attenuate Ca^{2+} accumulation in MACs triggered by Hcy, as well as abnormal electrical activity. In addition, Hcy increased the interaction between IP_3R1 and Nav1.5. These data suggest that Hcy induced Ca^{2+} accumulation is mediated by the IP_3R1/Nav1.5 signaling pathway, accompanied with the influx of Na^+ and Ca^{2+}, which act as triggers for electrical remodeling.

Keywords: Homocysteine, IP_3R1, Nav1.5, I_{NaL}, I_{CaL}, electrical remodeling

Introduction

Homocystine (Hcy) is a new cardiovascular injury factor, which plays a critical role in several pathological processes including oxidative stress, inflammation and cell apoptosis [1]. It was demonstrated that the levels of Hcy is closely related to the recurrence of atrial fibrillation (AF) after radiofrequency ablation [2]. Exposure to Hcy stimulates the development of electrical remodeling and reentrant circuit in atrium [3], which implies that Hcy is an independent risk factor for AF [4, 5]. Ca^{2+} events in atrial myocytes are hierarchical, from Ca^{2+} spark to small waves, and finally induce Ca^{2+} accumulation globally [9]. In addition, the activation of voltage gated L-type calcium channel (I_{CaL}) is indispensable for generating Ca^{2+} wave [6, 7]. When intracellular Ca^{2+} wave occurs, it subsequently activates IP_3Rs and cause Ca^{2+} accumulation via the interaction with other downstream proteins. Moreover, this process induces prolongation of action potential durations (APDs) and eventually triggers arrhythmogenesis. To decipher pathological mechanisms of atrial arrhythmia, it's critical in understanding whether Hcy increases I_{CaL} level and how IP_3R1 mediates Ca^{2+} signaling.

IP_3Rs, a Ca^{2+} channel localized on the sarcoplasmic reticulum (SR), exist as three subtypes (IP_3R1, IP_3R2, and IP_3R3) with distinct functional domains and biological functions [10, 11]. Previous studies have confirmed that increased expression of IP_3Rs in atrial myocytes were isolated from the left atrial appendage of chronic AF patients [12, 13]. However, it is not clear which subtype of IP_3Rs is involved in mechanism of atrial arrhythmias. IP_3R1 has a perinuclear distribution in the atrium, and shows elevated protein level in AF patients [14]. Although an early study showed that enhanced IP_3R2 expression was associated with enhanced susceptibility to arrhythmic diseases, IP_3R1 is likely to be a dominant protein for mediating Ca^{2+} signaling pathway in atrium. It may be because IP_3R1 conducts electricity from the atria to the ventricles and maintains communication between cells [15]. Furthermore, IP_3R1 is expressed at higher levels in atria than in ven-

tricles, and shows abundant perinuclear localization, mediating atrial hypertrophy.

Besides, it is well known that the electrical remodeling of atrial arrhythmic is closely related to the activity of both the Na^+ and Ca^{2+} currents involved in cardiac depolarization, which has an indispensable role in regulating action potential durations (APDs) [16, 29]. When Ca^{2+} influx via L-type Ca^{2+} currents (I_{CaL}) under Hcy stimulation, it induces the excessive Na^+ influx via the activation of Na^+/Ca^{2+} exchanger (NCX). Recently, it was confirmed that a mutation (F1759A) in the sodium channel (Nav1.5) could induce persistent Na^+ influx and late Na^+ currents (I_{NaL}), which causes spontaneous and sustained AF [17]. Moreover, increased Nav1.5 level was detected in the atrial myocytes of AF patients. Another study suggested that the phosphorylated Nav1.5 triggers delay afterdepolarizations (DAD) and/or early repolarization (EAD), which contributes to AF pathology [18]. Thus, we hypothesized that IP_3R1 interacts with Nav1.5, and IP_3R1/Nav1.5 signaling pathway mediates Hcy-induced Ca^{2+} accumulation in atrium.

Materials and methods

Isolation of cardiomyocytes

Adult mouse atrial cardiomyocytes (MACs) were isolated as previously described (Paknejad, & Hite, 2018). Briefly, 2.5% Uratan (0.6 ml/100 g) was injected intraperitoneally one hour. After euthanizing the mice, the hearts were rapidly removed after thoracotomy. After cannulation of the ascending aorta, the hearts were perfused with Ca^{2+}-free Tyrode's solution through the retrograde route (NaCl 136 mM, KCl 5.4 mM, $K_2HPO_4{\cdot}2H_2O$ 0.33 mM, $MgSO_4{\cdot}7H_2O$ 1.0 mM, HEPES 10 mM, and glucose 10 mM, pH = 7.4) at 37°C using a Langendorff apparatus. After 2-3 minutes of perfusion, an enzyme solution containing type II collagenase (Gibco Cat#:17101-015) 25 mg, BDM 25 mg, Carnitine 20 mg, Taurine 31 mg, L-Glutamic Acid 20 mg (1.66 mg/ml, Worthington Biomedical, Lakewood, NJ) in Ca^{2+}-free Tyrode's solution was perfused for 20 min (1.5 ml/min). Finally, the left atrial appendage was homogenized and filtered (200 μm) to make single cell suspension of cardiomyocytes, which were stored in KB (KOH 80 mM, KCl 30 mM, L-Glutamic Acid 50 mM, $MgCl_2$ 1 mM, HEPES 10 mM, Glucose 10 mM, KH_2PO_4 20 mM, Taurine 20 mM, EGTA 0.5 mM, pH = 7.4) following centrifugation. Cells were resuspended in 1 mM Ca^{2+}.

Cell models and treatment

MACs were cultured in DMEM (#11960051) (Gibco, CA, USA) supplemented with 10% fetal bovine serum (#10099-141) (Gibco, CA, USA). Groups: MACs treated with DMEM (control), MACs were treated with 500 μM (low-Hcy, LH) or 1 mM Hcy for 48 hours (High-Hcy, HH). In intervention group, 50 μM Nav1.5 inhibitor (eleclazine hydrochloride, ELE) was added for 8 hours into the control or HH group, called ELE, HH + ELE respectively. Simultaneously, 50 μM IP_3R1 inhibitor (2-aminoethoxydiphenyl borate, 2APB) was added into the control or HH group, called 2APB, HH + 2APB groups. For lentivirus experiments, MACs were injected with purified IP_3R1-knockdown (IP_3R1-shRNA) or Nav1.5-knockdown (Nav1.5-shRNA) lentivirus for 24 hours (MOI = 20), and treated with 1 mM Hcy, termed IP_3R1-shRNA + H or Nav1.5-shRNA + H groups. MACs were injected with scrambled lentivirus with or without Hcy treatment (Scramble, Scramble + H). ELE (HY-16738A) was purchased from MedChemExpress (USA), 2APB (AB-120124) was obtained from Abcam (Cambridge, UK). DL-Homocysteine (Hcy, H-4628) was obtained from Sigma-Aldrich (St. Louis, MO). ELE, 2APB and Hcy were dissolved in DMEM at 37°C.

Animal models

All animal experiments were approved by the SLAC Labomouseory Animal Co. Ltd, Hunan, China. Male C57B6 mice were maintained on a 12 h light/12 h dark cycle at a room temperature (20-25°C) at a relative humidity of 40-70%. Transthoracic echocardiography was performed and baseline information of the mice (n = 40) was recorded. WT-V mice were fed with high-Hcy diet (AIN-76A + 4% methionine with irradiation, ReadyDietech, China) to induce hyperhomocysteinaemia (WT-V + H, n = 10). Mice were injected with purified AAV-9 vectors (200 ul) [IP_3R1-shRNA or Nav1.5-shRNA] through the tail vein at one week of age, and designed as IP_3R1-knockdown (IP_3R1-KD) or Nav1.5-knockdown (Nav1.5-KD) respectively. Scrambled AAV9-vectors were injected as controls with or without a high-Hcy diet at four week of age (WT-V + H, WT-V). IP_3R1-KD or

Nav1.5-KD mice fed a high-Hcy diet were regarded as IP_3R1-KD + H, Nav1.5-KD + H groups, respectively. The study protocol was approved by the Institutional Review Board of the Second Affiliated Hospital of Nanchang University (Permit Number: 2016-022).

late sodium (I_{NaL}) recordings

I_{NaL} currents were assessed using a Port-a-Patch (Nanion Technologies, USA) connected to an EPC10-Quattro (Heka Instruments, Germany). Glass pipette with a tip resistance of 2- to 3.5-MΩ were used. Once gigaseal resistances were achieved, series resistance and cell-capacitance were compensated. Currents were elicited with 1000-ms pulses from a holding potential of -120 mV to 40 mV, applied at intervals of 10 mV. Myocytes were super-fused with buffer containing (mM): 140 mM NaCl, 5.4 mM CsCl, 1 mM $MgCl_2$, 1.8 mM $CaCl_2$, 0.3 mM $BaCl_2$, 10 mM glucose, 10 mM HEPES, 0.33 mM NaH_2PO_4, pH = 7.4 (NaOH). A Ca^{2+}-free pipette solution containing (mM): 120 mM CsCl, 10 mM TEA-Cl, 1 mM $CaCl_2$, 5 mM $MgCl_2$, 10 mM HEPES, 10 mM EGTA, 5 mM Na-ATP, pH = 7.2 (CsOH) were used. I_{Na} was detected from MACs, and I_{NaL} was measured before the ending of 200 ms pulsing after I_{Na} peak. Also note that for comparison purposes, I_{NaL} is expressed as normalized to cell size (in pA/pF).

L-type calcium currents

I_{CaL} was recorded using whole-cell voltage-clamping with an EPC10 Quattro amplifier (HEKA Ektronik, Germany) and Patchmaster software (HEKA Ektronik, Germany). A single cardiomyocyte was placed in the recording chamber equipped with an inverted microscope (IMT-2, Olympus, Tokyo, Japan), and super-fused with external solution (140 mM TEA-Cl, 2 mM $MgCl_2$, 10 mM $CaCl_2$, 10 mM HEPES, 5 mM Glucose, adjusted to pH 7.4 with TEA-OH) at a rate of 3 ml/min at 34 ± 1°C. Pipettes were filled with pipette solution [120 mM $CsCl_2$, 1 mM $MgCl_2$, 10 mM HEPES, 10 mM EGTA, 5 mM phosphocreatine disodium salt, 0.3 mM Na2-GTP, 4 mM Mg-ATP, adjusted to pH 7.2 with CsOH]. I_{CaL} was elicited by 11-step 500-ms depolarizing pulses with the test potentials in the range of -60 to 60 mV from a holding potential (HP) of -60 mV every 10 s. The amplitudes of the peak currents (pA) were normalized to cell membrane capacitance (pF).

Action potential duration recordings

APDs were recorded with standard intracellular microelectrodes in cardiomyocytes with or without Hcy stimulation. Induced APDs were measured using whole-cell current clamping. The external solution contained (in mM): 140 NaCl, 3.5 KCl, 1 $MgCl_2$, 2 $CaCl_2$, 10 Glucose, 10 HEPES, 1.25 NaH_2PO_4, pH = 7.4 (NaOH). The internal solution contained (in mM): 140 K-Gluconate, 5 NaCl, 0.1 $CaCl_2$, 1 $MgCl_2$, 10 HEPES, 1 EGTA, 2 Mg-ATP, pH adjusted to 7.2 with KOH. The following AP parameters were analyzed using the Patchmaster software (HEKA Ektronik, Germany): resting membrane potential (RMP), action potential amplitude (APA) and duration at 20%, 50% and 90% of repolarization (APD_{20}, APD_{50} and APD_{90}), and maximum upstroke velocity (d_V/d_{tmax}).

Intracellular Ca^{2+} concentrations ($[Ca^{2+}]_i$) in MACs

The intracellular Ca^{2+} concentration was measured using the fluo-4/AM probes (Sigma-Aldrich) and flow cytometry (BD, Franklin Lakes, USA). Cardiomyocyte suspensions were stained with 10 M by fluo-4/AM for 1 hr, and washed in PBS. Ca^{2+} concentrations were calculated using the formula: $[Ca^{2+}]_i$ (nM) = $K_d[(F-F_{min})/(F_{max}-F)]$. K_d: the dissociation constant (864 nM at 37°C). The fluorescence intensity of individual cells was recorded as the F value measured following the addition of 10 mM EGTA (20 μL) for 1 to 10 min, indicating the minimum fluorescence intensity, F_{min}. Finally, 10 g/L Triton X-100 and 1 mM $CaCl_2$ was added for 1 to 10 min to detect the maximum fluorescence intensity (F_{max}) (Ando, Kawaai, Bonneau, & Mikoshiba, 2018).

Adeno-associated virus (AAV) production and infection

AAV9-IP_3R1-mCherry tagged constructs targeting GGGAACATACGTCATT-ATTG at site 96 of *musculus* inositol 1,4,5-trisphosphate receptor 1 (NC_000072.6) or scrambled sequences were obtained from GeneCopoeia (Genomeditech, China). AAV9-Nav1.5-mCherry construct targeting GTATATGCAAATATGAAGGA at site 356 of *mus musculus* SCN5A (NC_000075.6) was also obtained. AAV9s were packaged in HEK293T cells using the triple transfection method, and purified using CsCl density gradient centrifugation. One-month old C57B6 mice

were injected with a single dose of AAV9-scrambled, AAV9-IP_3R1-shRNA, and AAV9-Nav1.5-shRNA virus (1.34×10^{12} VG/ml, 200 ul per mouse) via the caudal vein route, termed WT-V, IP_3R1-KD and Nav1.5-KD respectively. For AAV9 infected cell models, atrial myocytes were plated into T_{25} culture flasks at 4×10^3 cells/cm^2 and infected with AAV9-IP_3R1-shRNA, AAV9-Nav1.5-shRNA, or AA9-empty vector (scramble) at a multiplicity of infection of 20 (MOI = 20). Infection efficiencies (90-95%) were determined through the assessment of GFP fluorescence intensity.

Histopathological examination

Atrial tissues were fixed in 4% paraformaldehyde and embedded in paraffin wax. Samples were then stained with haematoxylin-eosin (H + E) and masson staining, both performed according to the manufacturer's instructions (Sigma-Aldrich). For electron microscopy, heart tissues were fixed with special fixative at 4°C for 2-4 h and rinsed 3 times with 0.1 M phosphate buffer (PB). Tissues were fixed with 1% osmium acid, rinsed with 0.1 M PB (pH = 7.4), and dehydrated with an ascending ethanol gradient for 15 min each time. Tissues were immersed in Epon812 resin/acetone (1:1) for 2-4 h, immersed in fresh Epon 812 resin for 30 min, and embedded for convergence overnight at 60°C. Samples were sectioned (60-80 nm thickness) using an ultrathin section machine, and subjected to uranium-lead double-staining (2% uranium acetate saturated alcohol solution, lead citrate, 15 min staining). Samples were imaged on a transmission electron microscope (HT-7700, Hitachi, Tokyo, Japan).

Immunofluorescence

For conventional fixation, cells were immersed in 4% polyoxymethylene and permeabilized in 0.1% Triton X-100. Cells were washed 3 times in sterile phosphate-buffered saline (PBS), and incubated with primary antibodies in PBS containing 5% bovine serum albumin (BSA) at 4°C overnight. Samples were washed 3 times in PBS, and stained with Alexa488- or 564-conjugated goat anti-rabbit/mouse secondary antibodies at room temperature for 1.5 h. Cell nuclei were stained with 4',6-diamidino-2-phenylindole (DAPI). Representative images were acquired using a BWS435 confocal microscope. LAS AF Lite software was used for professional image analysis (Zeiss, Germany).

qRT-PCR analysis

Heart tissues were stored in Allprotect Tissue Reagent (Qiagen, Hilden, Germany) for qRT-PCR analysis. Total RNA was isolated from heart tissue frozen in liquid nitrogen and extracted using TRIzol reagent (Invitrogen, MA). cDNA was synthesized from 2 μg of RNA using the PrimeScript™ 1st Strand cDNA Synthesis Kit (Takara Biomedical Technology, Dalian, China). Primers were obtained from Sangon Biotech (Shanghai, China) (IP_3R1, IP_3R2, IP_3R3, Nav1.5, RyR2). qRT-PCR was performed using SYBR® Premix Ex Taq™ (Tli RNaseH Plus) (Takara Biomedical Technology, Dalian, China) using the following conditions: 50°C for 2 min (UNG incubation), 95°C for 10 min (reverse transcription) and 40 cycles of 95°C for 5 sec (denaturation) and 60°C for 15 sec (annealing and extension); step three: dissociation protocol. Each cycle threshold (CT) value was normalized to the CT value of the housekeeping gene, GAPDH. Fold changes were calculated using the 2^(-ddCT) method compared to GAPDH. Expression levels were compared using log scale fold changes.

Western blot analysis

Proteins were extracted from heart tissue using a Tissue Homogenizer (PD500-TP12) (Prima, GBR) with RIPA lysis and extraction buffer supplemented with protease inhibitors (Thermo Fisher Scientific, MA). Protein concentration was quantified using BCA protein assay kits (Bio-Rad, CA) and 6-8% SDS-polyacrylamide gel electrophoresis (PAGE) was performed to resolve high-molecular-weight proteins (Solarbio, China), MES [2-morpholinoethane] SDS [sodium dodecyl sulfate] running buffer, transfer buffer and TBS [Tris buffered saline] Tween buffer were purchased from Life Technologies, CA. Anti-Nav1.5 and RyR2 antibodies were purchased from Abcam (Cambridge, UK; Nav1.5-ab56240 and RyR2-ab59225). Anti-IP_3R1 and anti-p-IP_3R1 (ser1756) antibodies were purchased from CST (Cell Signaling Technology, Boston, USA; IP_3R1-8568, p-IP_3R1-8548). GAPDH antibodies were obtained from Proteintech (Chicago, USA; GAPDH-60004-1-Ig). Membranes were probed with primary antibodies (1:500) in 5% BSA at 4°C and labeled with HRP-conjugated secondary antibodies (1:10,000) for 50 min in TBST at 37°C. Proteins were detected using a WESTAR ETA C ULTRA 2.0 (Cyanagen, ITA). Images were evaluated

using a ChemiDoc MP imaging system (Bio-Rad, CA).

Results

Hcy triggers the electrical remodeling in the atrial myocytes, following with Na^+ and Ca^{2+} influx

Figure 1A showed that compared to control group, the HH group produced maximal amplitude of I_{CaL}, but it showed only small changes in the LH group without statistical significant. The voltage-dependent steady state activation (SSA) of I_{CaL} showed a leftward shift in the HH group [**Figure 1Ad**]. Moreover, the open probability of I_{CaL} ($V_{1/2}$) in SSA increased in the HH group, whilst the voltage sensitivity of I_{CaL} (K_a value) in SSA and steady state inactivation (SSI) remained unaltered in the above three groups, as well as the $V_{1/2}$ in SSI [**Figure 1Ad**, **Figure 1Ae**; **Table 1A**]. Intracellular $[Ca^{2+}]_i$ level was detected higher in the HH group than that in the LH group (**Figure 1B**). On the other hand, the results revealed that I_{NaL} was significantly up-regulated in the HH group (**Figure 1C**). Finally, the effects of Hcy in the I_{caL} parameters were also recorded (**Table 1**). Even though Hcy stimulation produced no obvious effects on the APD_{50} and APA (**Table 2A**), Hcy increased dV/dt_{max} value, and prolonged APD_{90}. These effects were more prominent in the HH groups, with the LH group showing slightly changes (**Figure 1D**; **Table 2A**).

IP_3R1 and Nav1.5 both contribute to modulate electrical remodeling under Hcy stimulation

In MACs, even if Hcy triggers the Na^+ and Ca^{2+} influx, 2APB and ELE both reduced the characteristic index of I_{NaL} and I_{CaL}, including the decreased $V_{1/2}$ and Ki levels of I_{CaL} in SSA, and lower I_{NaL} current densities (**Figure 2A**, **2E**; **Table 1A**). In animal model, the maximal amplitude of I_{CaL} and the index in SSA were attenuated in IP_3R1-KD + H or Nav1.5-KD + H mice in comparison with that in the WT-V + H group (**Figure 2B**, **Table 1B**). Furthermore, 2APB and ELE both effectively alleviated the enhanced $[Ca^{2+}]_i$ level in response to Hcy stimulation (**Figure 2C**). Interestingly, *in vivo and in vitro*, the inhibitory effect of IP_3R1 on $[Ca^{2+}]_i$ level was slightly apparent than that of Nav1.5 (**Figure 2C**, **2D**). Moreover, the animal experiments demonstrated that enhanced I_{NaL} current densities was alleviated in IP_3R1 or Nav1.5 blocking models (**Figure 2F**). Above evidence suggested that IP_3R1 and Nav1.5 proteins contributed to $[Ca^{2+}]_i$ accumulation, which was mainly attributed to the elevated levels of I_{CaL} and I_{NaL}. In addition, 2APB and ELE alleviated the APD_{90} prolongation and the upstroke velocity of dV/d_{tmax} induced by Hcy (**Figure 2G**; **Table 2B**). Similarly, these effects were inhibited in the IP_3R1-KD + H or Nav1.5-KD + H groups (**Figure 2H**). Interestingly, the effect of blocking APD was greater in IP_3R1-KD model than in Nav1.5-KD model [**Figure 2H**; **Table 2C**], suggesting that IP_3R1 is a more significant contributor to affect APD functions. However, APD_{20}, APD_{50} and APA showed minimal changes between the control, the LH and the HH groups (**Table 2A**).

Enhanced IP_3R1 promotes Nav1.5 activity under Hcy stimulation

As shown in **Figure 3A**, Hcy stimulation led to a dose-dependent increase in the expression protein of IP_3R1 and Nav1.5. 2APB could blunt the effect of high Hcy in the expression of Nav1.5 protein (**Figure 3B**). However, enhanced IP_3R1 level was not altered after ELE treatment. Similarly, *in vivo experiment*, showed that the up-regulated levels of IP_3R1 and Nav1.5 were mitigated in IP_3R1-shRNA cells, but enhanced level of IP_3R1 maintained in Nav1.5-shRNA cells (**Figure 3C**, **3D**). *In vitro experiment,* **Figure 3E** outlines the procedure of injecting purified AAV-9 into mice. We used confocal microscopy and WB analysis to confirm the efficiency of AAV9 transfection (**Figures 3F**, S2A-C). The effect of Hcy was completely inhibited in the IP_3R1-KD + H mice, compared to the WT-V + H mice (**Figure 3G**). After Hcy stimulation, ryanodine receptors 2 (RyR2), as the other modulator of Ca^{2+} in ER, was detected a decreased protein level (**Figure 3A**). However, the effect of Hcy in the protein level of RyR2 could be alleviated by the inhibition of IP_3R1 (**Figure 3B-D**, **3G**). Interestingly, although the levels of phosphorylated IP_3R1 (p-IP_3R1, S1756 domain) were down-regulated under Hcy stimulation, the levels of p-IP_3R1 were enhanced in the situation of inhibiting Nav1.5 gene (**Figure 3B-D**), in accordance with the result of animal experiment (**Figure 3F**, **3G**).

IP_3R1 is a Nav1.5-interacting partner

After Hcy treatment for 48 hrs, IP_3R1/p-IP_3R1 and Nav1.5 co-localized (**Figure 4A-C**). Although

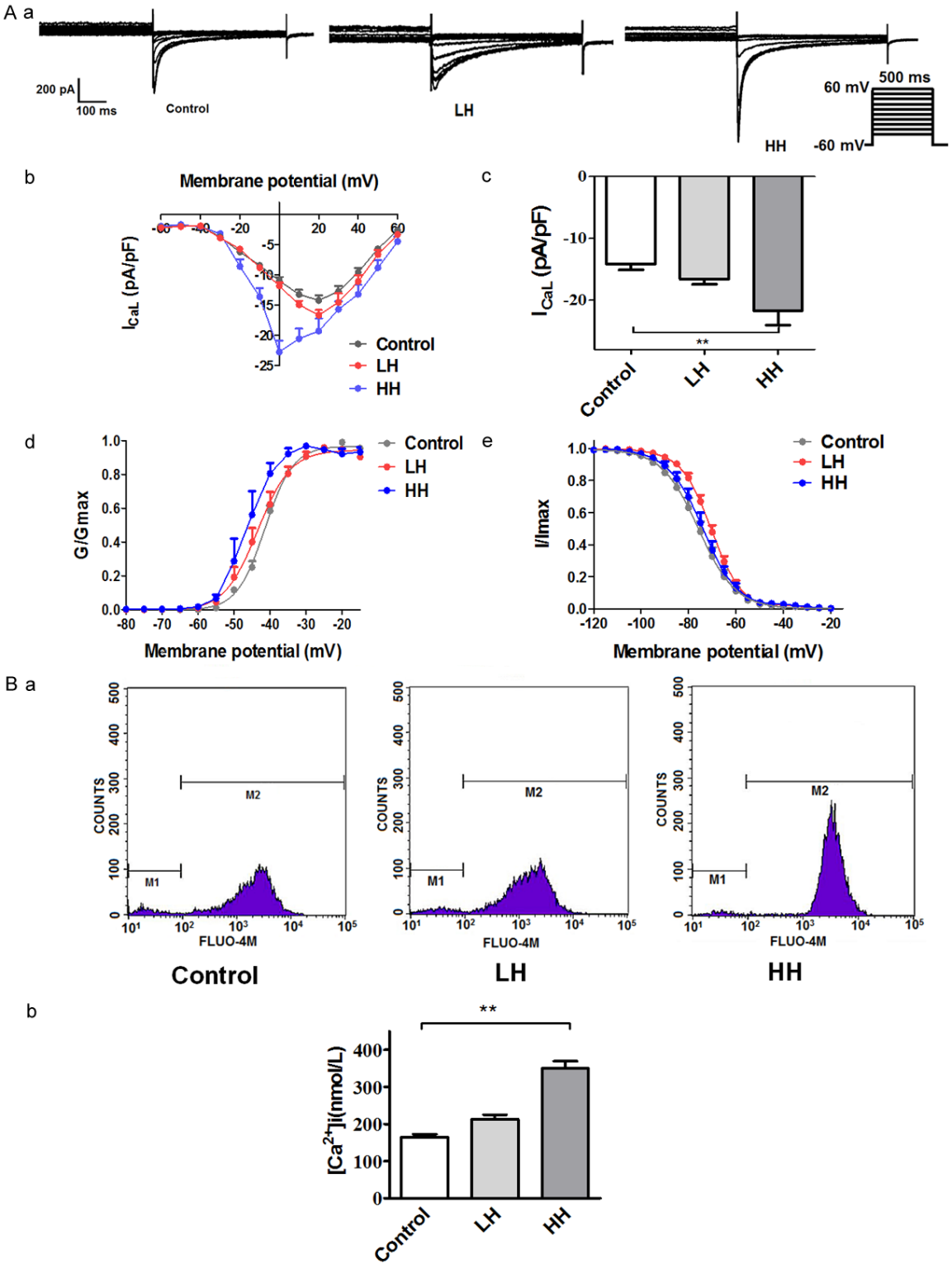
A a
200 pA
100 ms
Control
LH
HH
60 mV
500 ms
-60 mV
b
Membrane potential (mV)
I_{CaL} (pA/pF)
Control
LH
HH
c
I_{CaL} (pA/pF)
**
Control
LH
HH
d
G/Gmax
Membrane potential (mV)
Control
LH
HH
e
I/Imax
Membrane potential (mV)
Control
LH
HH
B a
COUNTS
FLUO-4M
M1
M2
Control
LH
HH
b
**
$[Ca^{2+}]i$(nmol/L)
Control
LH
HH

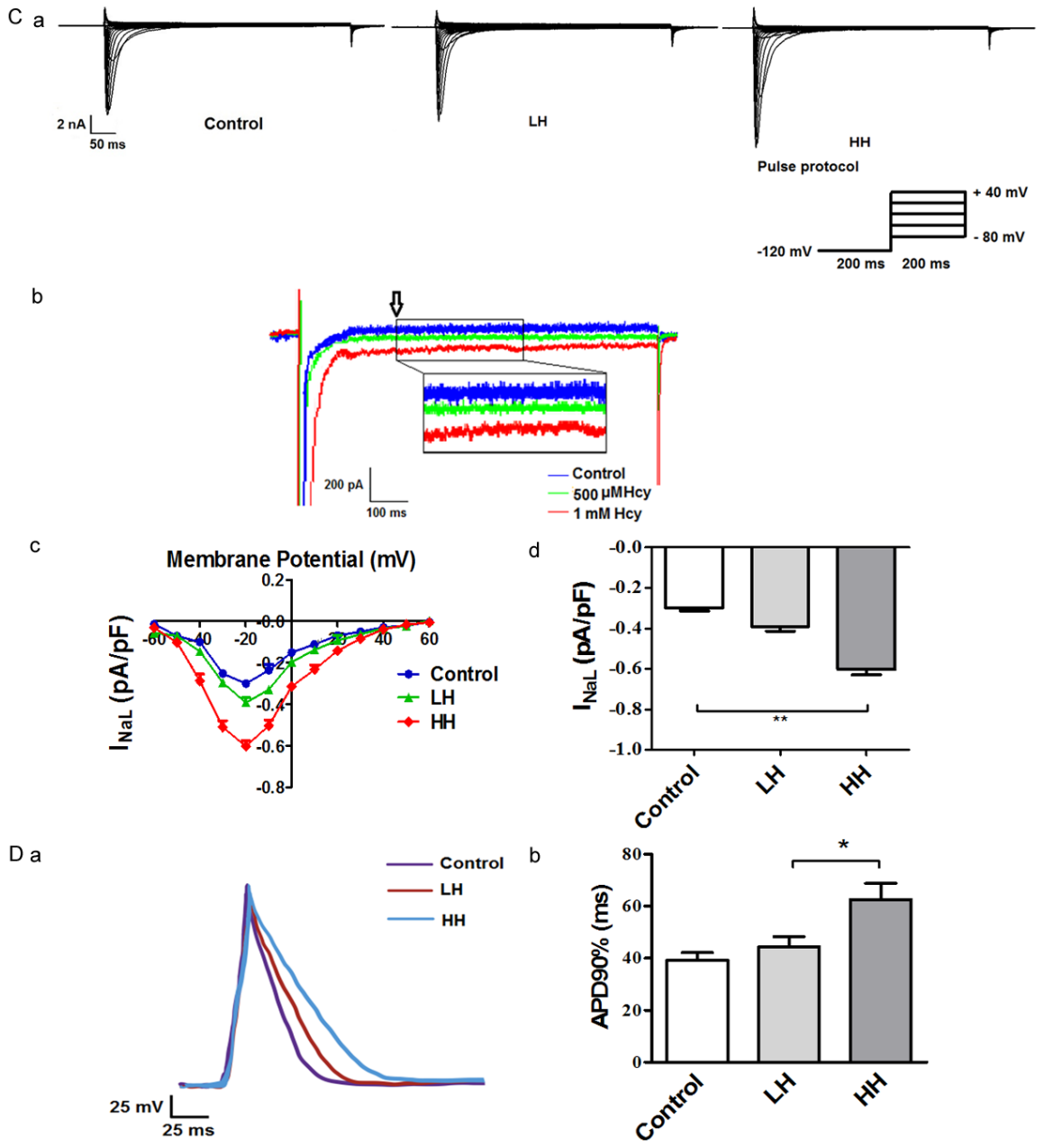

Figure 1. MACs treated with high concentration of Hcy (1 mM, HH group) cause significant increase in I_{CaL}, and I_{NaL} density (A, C) in wide range of membrane potentials and prolongation of action potential duration (D), compared to the control group, as well as enhanced $[Ca^{2+}]_i$ level (B). (A) I_{CaL} currents recorded in the presence of low (500 μM, LH) and high Hcy (1 mM, HH) concentration following 48 h treatment. Representative I_{CaL} recordings (a), I-V curves of I_{CaL} and summary data (b, c), Steady-state activation (d) and inactivation (e) curves of I_{CaL} (mean ± SEM, n = 6). (B) Fluorescence intensity curves (a) and analysis of $[Ca^{2+}]_i$ (b) (mean ± SEM, n = 4). (C) (a) Representative late sodium current (I_{NaL}) recordings; (b) Measurement of I_{NaL} in atrial myocytes at voltages between -120 mV to +40 mV (measured as before the ending of 200 ms pulsing after peak, indicated by black arrows); (c, d) Summary of normalized I_{NaL} magnitude in control, LH and HH groups (mean ± SEM, n = 8). (D) (a, b) Superimposed recordings of optical action potentials and APDs at 90% of repolarization (APD_{90}) (mean ± SEM, n = 8 per treatment group). One-way analysis of variance (ANOVA) was applied to calculate all statistical significance with the exception of (B) (b), where were analyzed by student' s t-test.

stronger nuclear localization between Nav1.5 and IP_3R1 was observed under Hcy stimulation [**Figure 4A**, **4Ca**], the interaction between p-IP_3R1 and Nav1.5 decreased under Hcy stim-

Table 1A. Properties of CaV1.2 currents from MACs with or without 2APB, ELE

	Control	HH (1 mM)	2APB (50 μM)	ELE (50 μM)	H + 2APB	H + ELE
I-V relationship						
Peak current density (pA/pF)	-8.99 ± 3.30 (10)	-18.25 ± 4.85*** (7)	-6.88 ± 2.70 (8)	-10.52 ± 3.01 (7)	-9.28 ± 2.25## (6)	-11.78 ± 2.53# (7)
Voltage-dependent activation						
$V_{1/2}$ act (mV)	4.53	-5.91**	5.81	5.30	2.39##	0.13#
Slope (K_a value)	11.06	10.53	9.98	14.81	13.68	11.39
Voltage-dependent inactivation						
$V_{1/2}$ act (mV)	-22.80	-20.55	-22.99	-21.64	-24.06	-26.29
Slope (K_i value)	5.99	-5.50	6.97	7.36	5.68	-6.73

Numbers in parenthesis indicate experimental number. **P<0.01, ***P<0.001 when compared to control; #P<0.05, ##P<0.01, when compared to HHcy.

Table 1B. Properties of CaV1.2 currents from MACs in IP_3R1-KD or Nav1.5-KD mice

	WT-V	WT-V + H	IP_3R1-KD + H	Nav1.5-KD + H
I-V relationship				
Peak current density (pA/pF)	-7.01 ± 2.36 (4)	-15.88 ± 1.97*** (5)	-11.20 ± 3.07## (7)	-12.56 ± 3.52# (5)
Voltage-dependent activation				
$V_{1/2}$ act (mV)	1.70	-7.68*	-2.83#	3.49#
Slope	13.93	14.64	10.34	13.11
Voltage-dependent inactivation				
$V_{1/2}$ act (mV)	-24.14	-19.55	-20.85	-23.15
Slope	6.97	-6.89	6.77	-7.025

Numbers in parenthesis indicate experimental number. *P<0.05, ***P<0.0001 when compared to WT-V; #P<0.05, ##P<0.01 when compared to WT-V + H.

Table 2A. Effects of Hcy on action potential parameters (1 Hz) from MACs, n = 8

AP parameter	Control	Hcy	
		500 μM	1000 μM
APD_{90} (ms)	43.07 ± 9.78	46.89 ± 13.09	62.54 ± 17.58*
APD_{50} (ms)	12.42 ± 4.74	12.97 ± 3.53	15.13 ± 4.01
APD_{20} (ms)	5.74 ± 1.91	6.07 ± 1.51	5.73 ± 1.06
APA (mV)	125.2 ± 14.94	136.1 ± 17.15	143.1 ± 5.88
RMP	-76.85 ± 1.79	-80.42 ± 3.98	-78.91 ± 2.92
dV/dt_{max} (V/s)	152.6 ± 42.43	216.3 ± 58.86	251.6 ± 68.54**

*P<0.05, **P<0.01 when compared to control.

ulation due to the decreased p-IP_3R1 level in the HH groups [**Figure 4B**, **4Cb**]. Above results suggest that the interaction between IP_3R1 and Nav1.5 markedly increases under Hcy stimulation, both of which mediate the signaling pathways of electrical remodeling in atrium.

Inhibition IP_3R1/Nav1.5 axis alleviate Hcy-induced the damage in atrial myocytes

Even though it was under Hcy stimulation, the electrical remodeling could be efficiently alleviated via inhibition of IP_3R1/Nav1.5 signaling pathway, including Ca^{2+} and Na^+ influx, and APD prolongation (**Figures 1**, **2**). Structural remodeling was evaluated by observing at the ultrastructure of atrial tissue via electron microscopy, which detected rupture of the fascicle, loose arrangements of both crude and fine filaments, hyperplasia, and disordered mitochondrial cristae (Figure S3A). As noted by masson staining, Hcy-induced fibrosis were blocked in IP_3R1-KD + H and Nav1.5-KD + H mice, as well as the degree of nuclear deformation, when it was compared to WT-V + H mice (Figure S3B). Meanwhile, the IP_3R1/Nav1.5 knockdown mice displayed no apparent changes in cardiac size, even if it was under Hcy stimulation (Figure S3C).

Discussion

Although a large number of prior studies have demonstrated that Hcy is closely associated with the pathological mechanism of arrhythmic disease, especially AF [19], the underlying signaling pathway of electrical remodeling in the

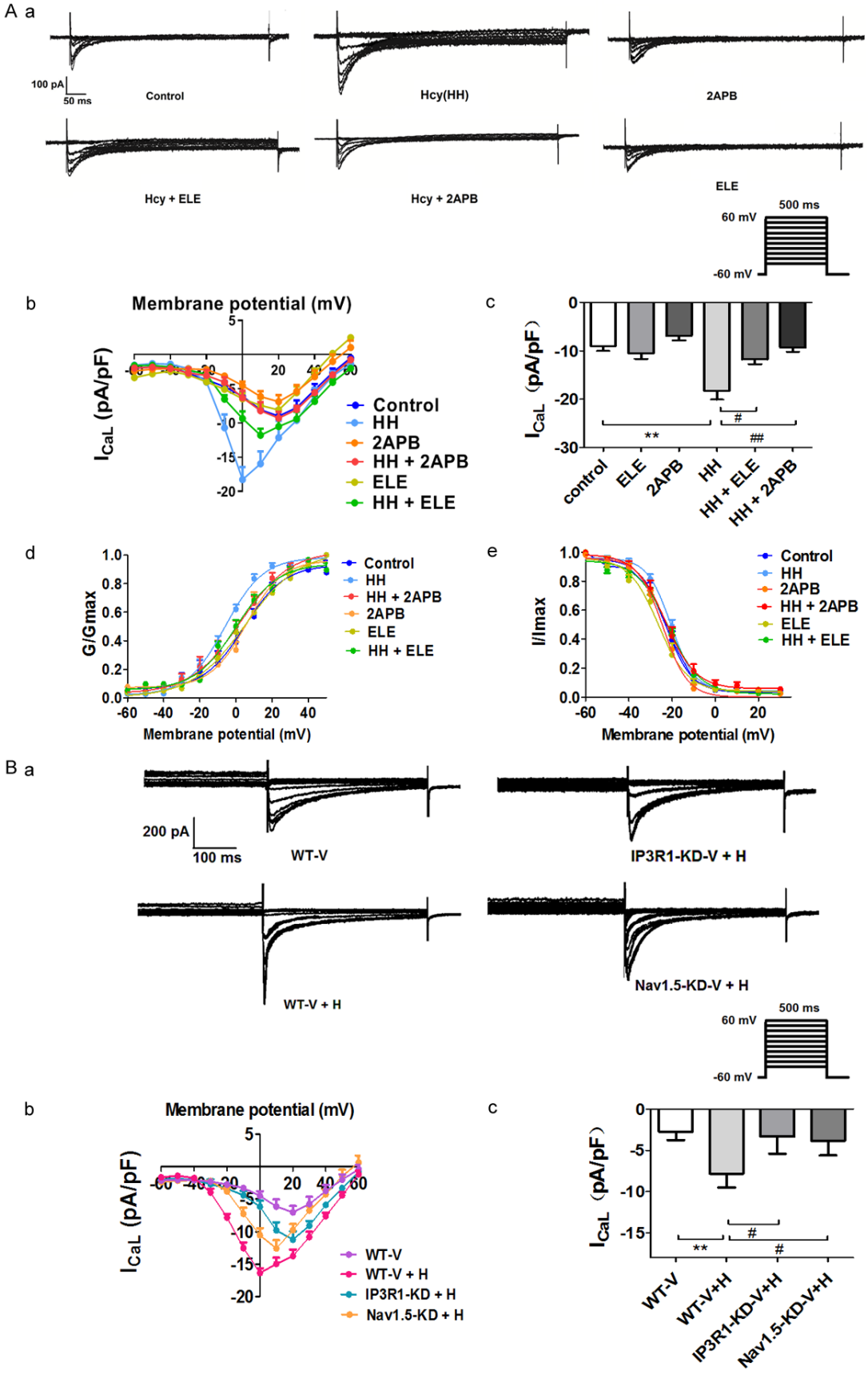
A a
100 pA
50 ms
Control
Hcy(HH)
2APB
Hcy + ELE
Hcy + 2APB
ELE
500 ms
60 mV
-60 mV
b
Membrane potential (mV)
I_CaL (pA/pF)
Control
HH
2APB
HH + 2APB
ELE
HH + ELE
c
I_CaL (pA/pF)
**
#
##
control
ELE
2APB
HH
HH + ELE
HH + 2APB
d
G/Gmax
Membrane potential (mV)
e
I/Imax
Membrane potential (mV)
B a
200 pA
100 ms
WT-V
IP3R1-KD-V + H
WT-V + H
Nav1.5-KD-V + H
500 ms
60 mV
-60 mV
b
Membrane potential (mV)
I_CaL (pA/pF)
WT-V
WT-V + H
IP3R1-KD + H
Nav1.5-KD + H
c
I_CaL (pA/pF)
**
#
#
WT-V
WT-V+H
IP3R1-KD-V+H
Nav1.5-KD-V+H

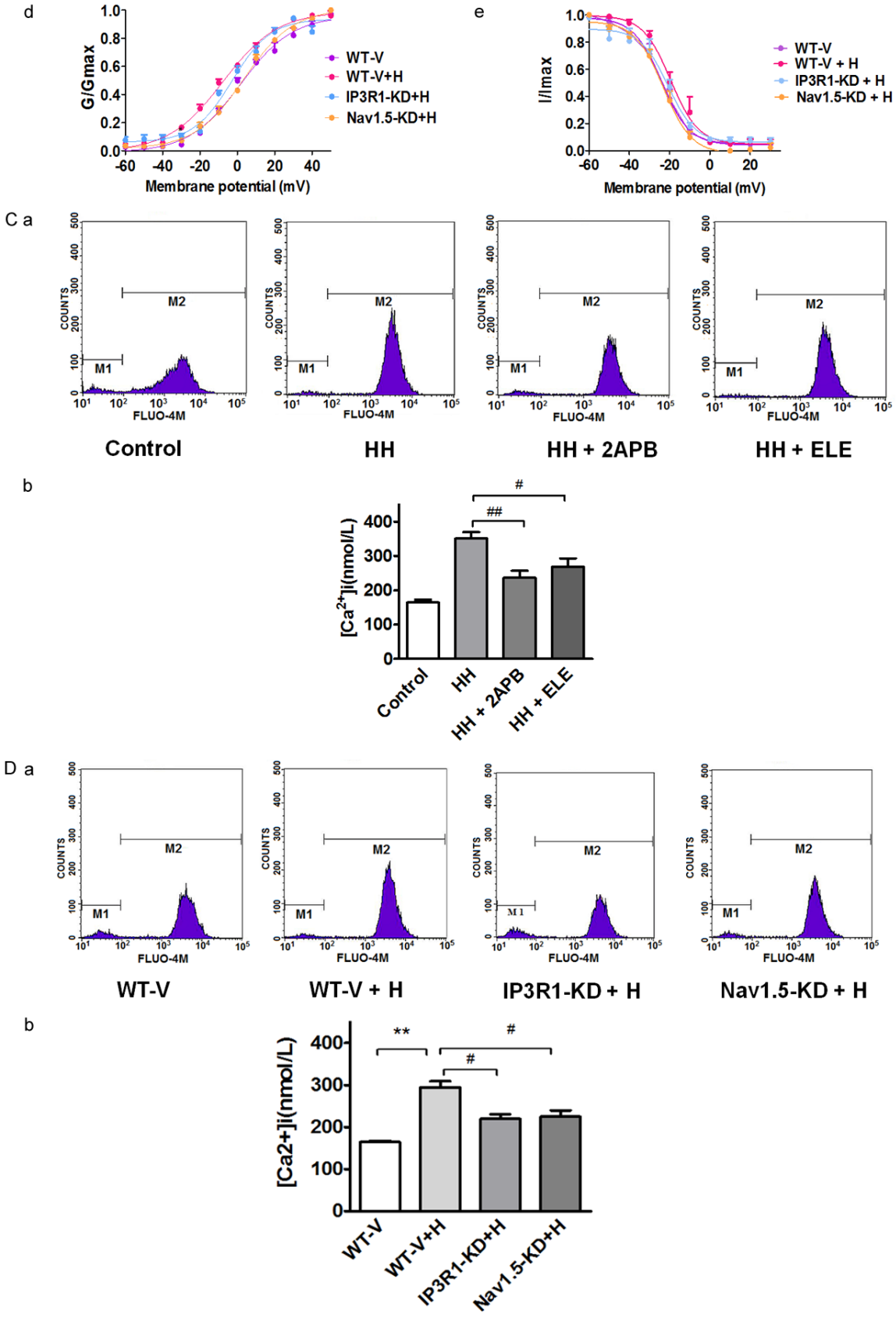
d
G/Gmax
Membrane potential (mV)
WT-V
WT-V+H
IP3R1-KD+H
Nav1.5-KD+H
e
I/Imax
Membrane potential (mV)
WT-V
WT-V + H
IP3R1-KD + H
Nav1.5-KD + H
C a
COUNTS
FLUO-4M
M1
M2
Control
HH
HH + 2APB
HH + ELE
b
[Ca2+]i(nmol/L)
Control
HH
HH + 2APB
HH + ELE
D a
WT-V
WT-V + H
IP3R1-KD + H
Nav1.5-KD + H
b
[Ca2+]i(nmol/L)
WT-V
WT-V+H
IP3R1-KD+H
Nav1.5-KD+H

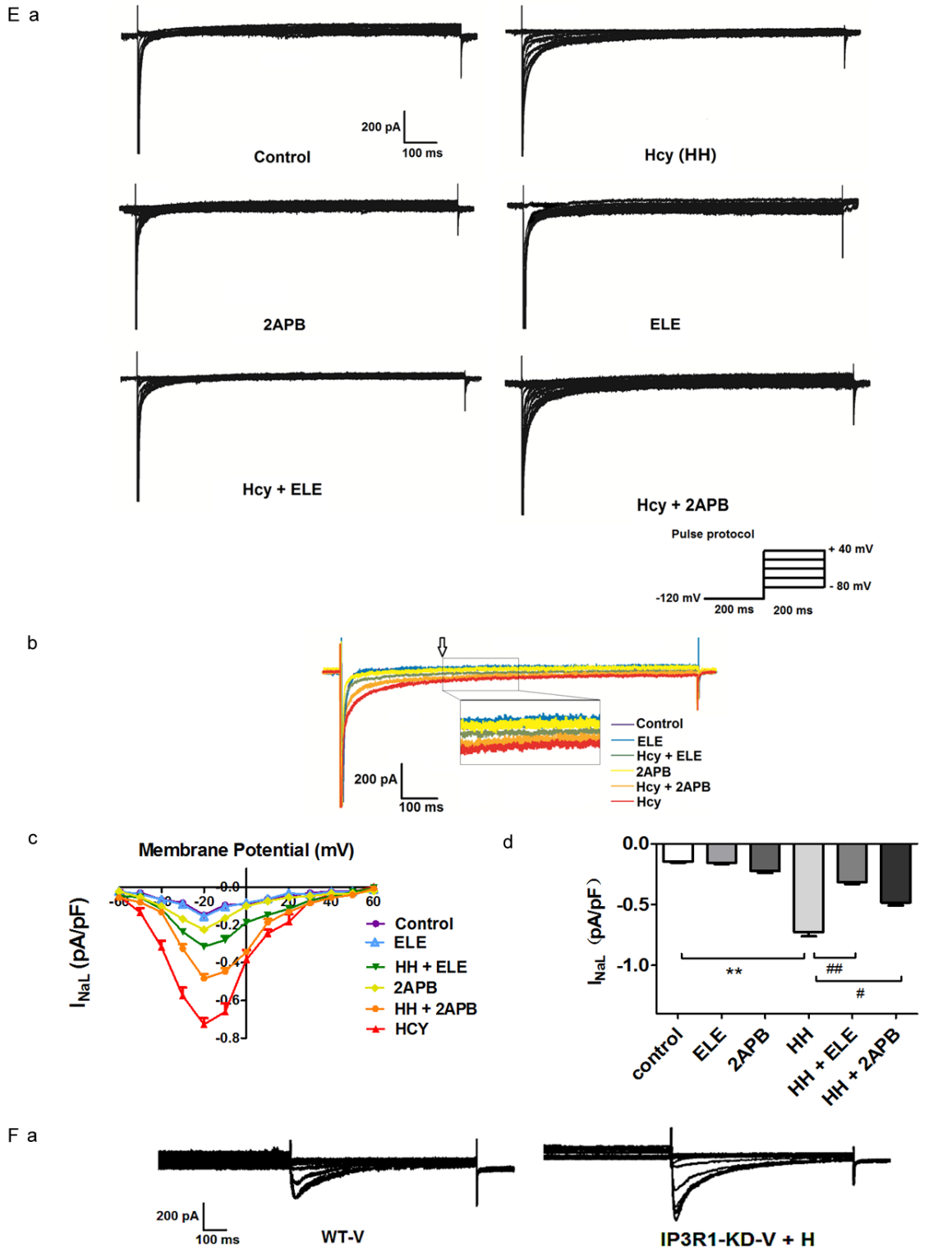
E a
200 pA
100 ms
Control
Hcy (HH)
2APB
ELE
Hcy + ELE
Hcy + 2APB
Pulse protocol
+ 40 mV
- 80 mV
-120 mV
200 ms
200 ms
b
Control
ELE
Hcy + ELE
2APB
Hcy + 2APB
Hcy
200 pA
100 ms
c
Membrane Potential (mV)
INaL (pA/pF)
Control
ELE
HH + ELE
2APB
HH + 2APB
HCY
d
INaL (pA/pF)
0.0
-0.5
-1.0
**
##
#
control
ELE
2APB
HH
HH + ELE
HH + 2APB
F a
200 pA
100 ms
WT-V
IP3R1-KD-V + H

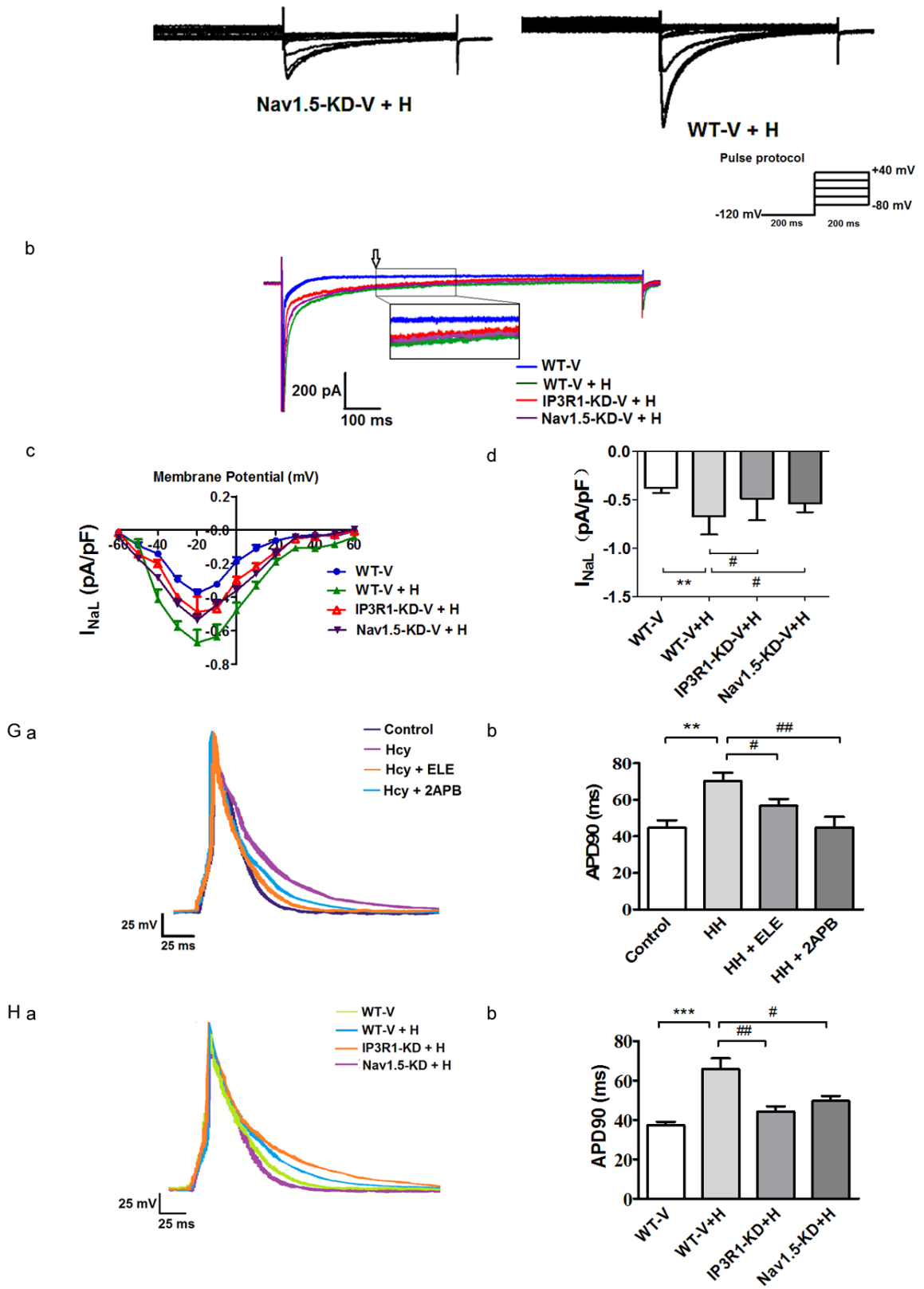

Figure 2. Inhibition of Nav1.5 or IP_3R1 can efficiently alleviate the effect of high concentration of Hcy *in vitro and in vivo*, including the reduction in I_{CaL}, and I_{NaL} density (A, B, E, F), lower $[Ca^{2+}]_i$ level (C, D), and reduction of APD (G, H). (A) Representative I_{CaL} recordings (a), I-V curves of I_{CaL} and summary data (b, c), Voltage-dependent current activation (d) or inactivation curves (e) of I_{CaL} (mean ± SEM, n = 8). (B) I-V curves of I_{CaL} (a) and Maximal I_{CaL} of I-V curves (b).

(B) Representative I_{CaL} recordings (a), I-V curves of I_{CaL} and summary data (b, c), Voltage-dependent current activation (d) or inactivation curves (e) of I_{CaL} (mean ± SEM, n = 8). (C) Fluorescence intensity curves (a) and analysis of intracellular Ca^{2+} concentration (b) (mean ± SEM, n = 4). (D) Fluorescence intensity curves (a) and the analysis of intracellular Ca^{2+} concentrations (b) (mean ± SEM, n = 4). (E and F) (a) Representative late sodium current (I_{NaL}) recordings; (b) Measurement of I_{NaL} in atrial myocytes at voltages between -120 mV to +40 mV (measured as before the ending of 200 ms pulsing after peak, indicated by black arrows); (E) (c, d) Summary of normalized I_{NaL} magnitude (mean ± SEM, n = 6). (F) (c, d) Summary of normalized I_{NaL} magnitude (mean ± SEM, n = 3). (G) (a) Superimposed recordings of optical action potential traces recorded in MACs; (b) Summary data from experiments as in panel a (mean ± SEM, n = 6). (H) (a) Superimposed recordings of optical action potential traces (mean ± SEM, n = 6); (b) Summary data from experiments as in panel a (mean ± SEM, n = 6). ANOVA was been applied to all statistical significance with the exception of (Cb), (Db), where were analyzed by student' s t-test.

Table 2B. Effects of ELE or 2APB on action potential parameters (1 Hz) from MACs, n = 6

AP parameter	Control	Hcy (1 mM)		
		Saline	ELE (50 μM)	2APB (50 μM)
APD_{90} (ms)	44.70 ± 9.97	70.15 ± 11.47*	56.61 ± 9.21#	44.74 ± 14.63##
APD_{50} (ms)	11.69 ± 5.64	16.36 ± 3.67	13.94 ± 6.79	12.99 ± 4.35
APD_{20} (ms)	5.90 ± 1.45	6.03 ± 1.43	5.67 ± 0.44	5.52 ± 4.94
APA (mV)	129.8 ± 12.08	140.4 ± 4.32	136.5 ± 10.04	132.5 ± 18.37
RMP	-77.96 ± 2.08	-79.83 ± 2.62	-76.95 ± 4.35	-83.56 ± 7.03
dV/dt_{max} (V/s)	156.2 ± 35.70	274.1 ± 85.44**	217.1 ± 38.87	185.3 ± 28.84#

*P<0.05, **P<0.01 when compared to control; #P<0.05, ##P<0.01, when compared to HHcy.

Table 2C. Effects of inhibiting IP_3R1 or Nav1.5 on action potential parameters (1 Hz) from MACs, n = 6

AP parameter	WT-V	Hcy (1 mM)		
		WT-V	IP_3R1-KD	Nav1.5-KD
APD_{90} (ms)	40.61 ± 7.52	62.34 ± 14.42**	46.68 ± 8.20#	51.61
APD_{50} (ms)	10.37 ± 2.75	12.47 ± 4.67	12.36 ± 2.75	13.64 ± 2.80
APD_{20} (ms)	4.86 ± 3.20	5.52 ± 1.49	6.87 ± 3.43	4.72 ± 2.86
APA (mV)	147.3 ± 23.57	158.4 ± 22.54	136.7 ± 12.91	146.7 ± 19.37
RMP	-76.85 ± 1.79	-78.91 ± 2.92	-80.42 ± 3.98	-83.57 ± 1.58
dV/dt_{max} (V/s)	165.4 ± 21.36	226.6 ± 22.15**	198.3 ± 21.40#	191.5 ± 28.04#

**P<0.01 when compared to WT-V; #P<0.05, ##P<0.01, when compared to WT-V + H.

atrium remains to be investigated. Abnormal $[Ca^{2+}]_i$ homeostasis is closely associated with the process of cardiac arrhythmias. It was also confirmed that the silence of subcellular Ca^{2+} signaling alleviates atrial tachycardia, especially AF [20]. Therefore, the signaling pathways of modulating Ca^{2+} homeostasis play an indispensable role in the pathological mechanisms of arrhythmias. Previous study affirmed that IP_3Rs is the predominant intracellular Ca^{2+}-release channel that conducts electrical signals from the atria to the ventricles [21]. Up to 50% of chronic AF patients have been detected to have an increased IP_3Rs level in atrial myocytes [22]. Multiple studies have shown that the frequency of IP_3-induced Ca^{2+} events in AF patients is significantly higher than that in the patients with sinus rhythm [23, 24]. In this study, we demonstrated that the mRNA level of IP_3R1 isoform was enhanced in the atrium of AF patients with hyperhomocysteinemia, but it appeared no significant change in the mRNA levels of IP_3R2 or IP_3R3 (Figure S1). Therefore, we focus on how Hcy affects Ca^{2+} homeostasis via the IP_3R1 signaling pathway in atrium.

It is well known that the formation of Ca^{2+} wave is due to the opening of I_{CaL}, and subsequently trigger Na^+ influx via the NCX activation reversely. Interestingly, Na^+ influx via increased I_{NaL} currents could induce global Ca^{2+} accumulation in intracellular, which was considered as a pro-

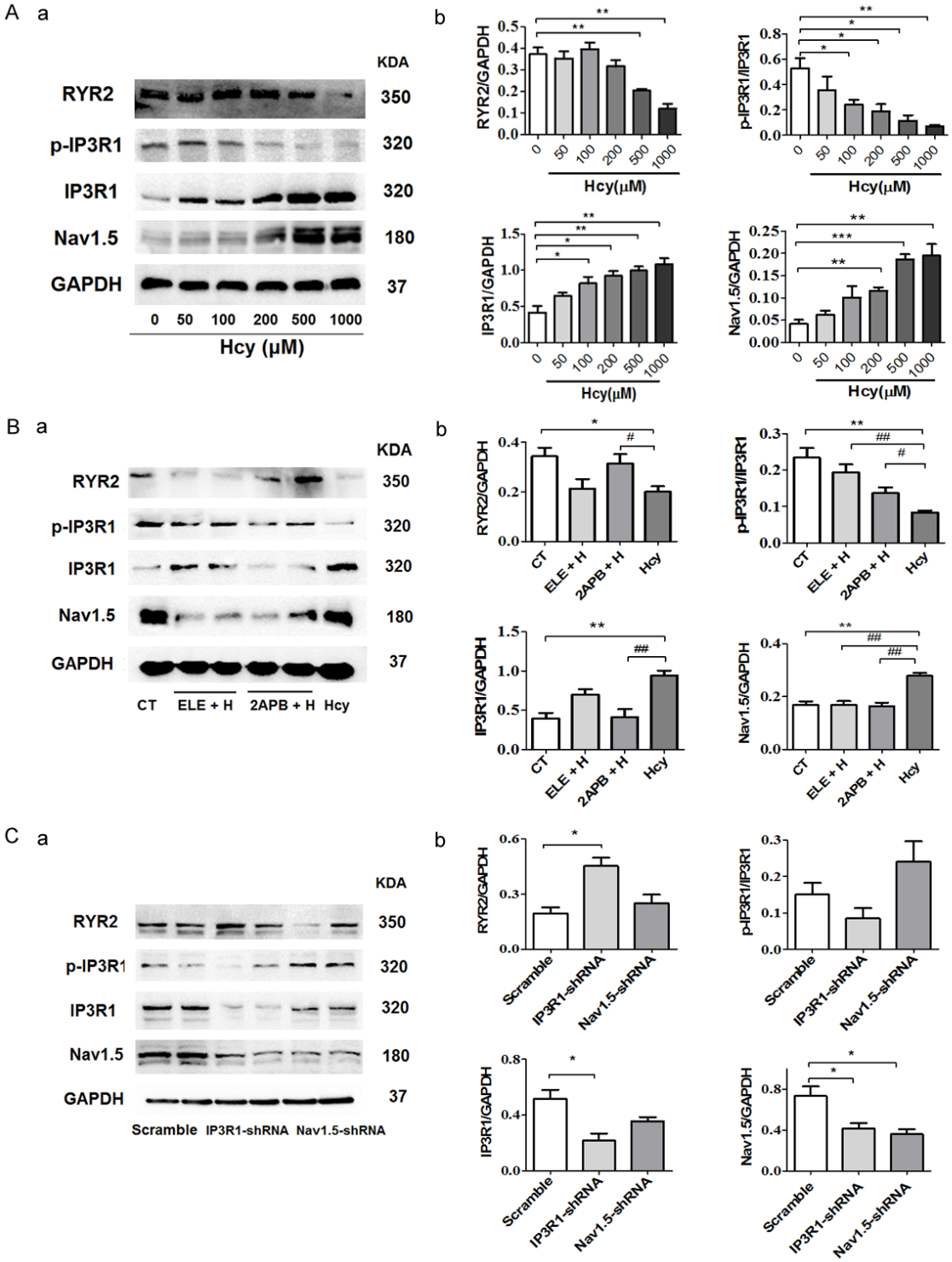
A a
KDA
RYR2
350
p-IP3R1
320
IP3R1
320
Nav1.5
180
GAPDH
37
0 50 100 200 500 1000
Hcy (μM)
b
RYR2/GAPDH
p-IP3R1/IP3R1
IP3R1/GAPDH
Nav1.5/GAPDH
Hcy(μM)
B a
KDA
RYR2
350
p-IP3R1
320
IP3R1
320
Nav1.5
180
GAPDH
37
CT
ELE + H
2APB + H
Hcy
b
RYR2/GAPDH
p-IP3R1/IP3R1
IP3R1/GAPDH
Nav1.5/GAPDH
C a
KDA
RYR2
350
p-IP3R1
320
IP3R1
320
Nav1.5
180
GAPDH
37
Scramble
IP3R1-shRNA
Nav1.5-shRNA
b
RYR2/GAPDH
p-IP3R1/IP3R1
IP3R1/GAPDH
Nav1.5/GAPDH

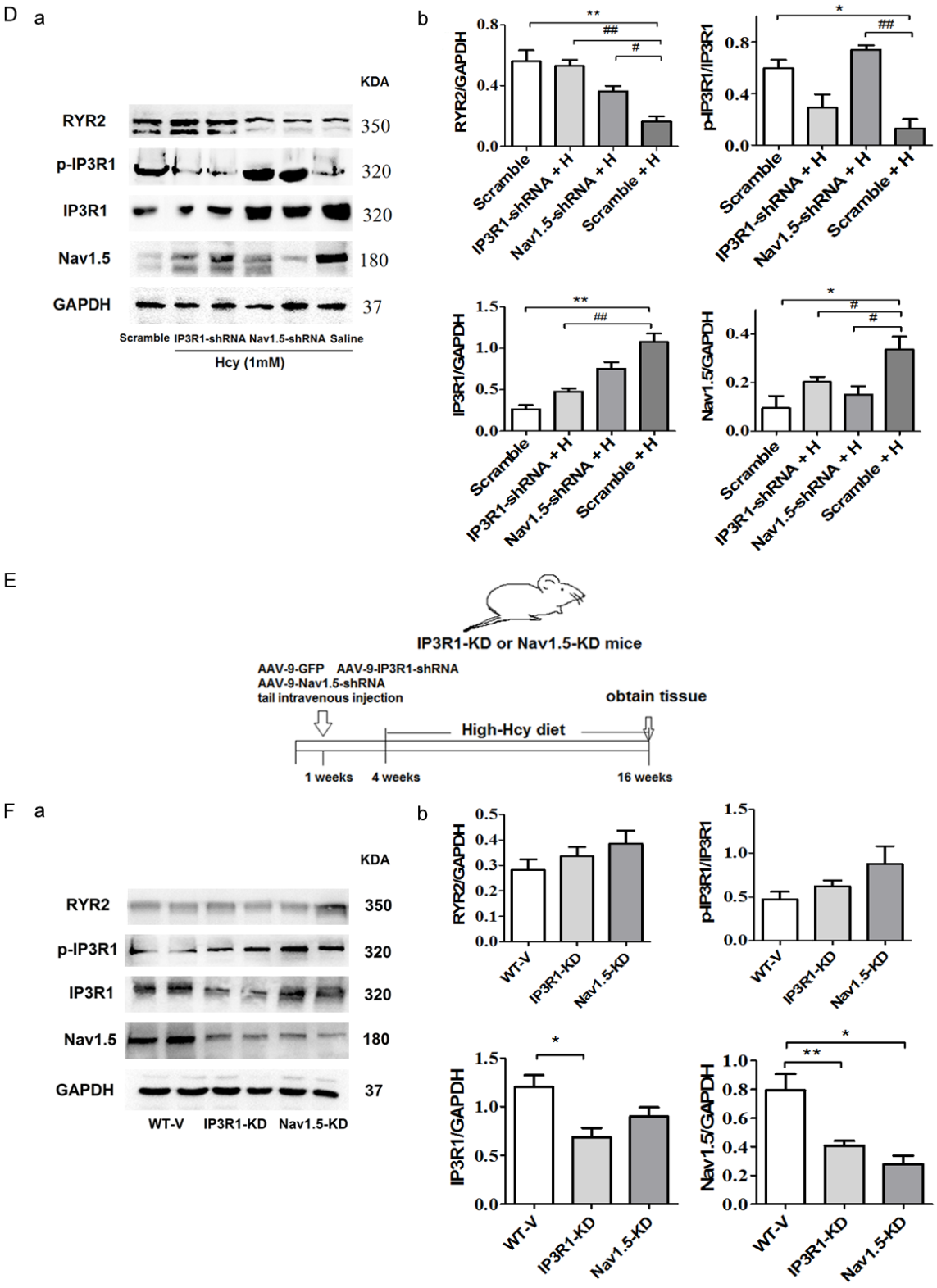
D
a
KDA
RYR2
p-IP3R1
IP3R1
Nav1.5
GAPDH
350
320
320
180
37
Scramble
IP3R1-shRNA
Nav1.5-shRNA
Saline
Hcy (1mM)
b
RYR2/GAPDH
p-IP3R1/IP3R1
IP3R1/GAPDH
Nav1.5/GAPDH
Scramble
IP3R1-shRNA + H
Nav1.5-shRNA + H
Scramble + H
E
IP3R1-KD or Nav1.5-KD mice
AAV-9-GFP
AAV-9-IP3R1-shRNA
AAV-9-Nav1.5-shRNA
tail intravenous injection
obtain tissue
High-Hcy diet
1 weeks
4 weeks
16 weeks
F
a
KDA
RYR2
p-IP3R1
IP3R1
Nav1.5
GAPDH
350
320
320
180
37
WT-V
IP3R1-KD
Nav1.5-KD
b
RYR2/GAPDH
p-IP3R1/IP3R1
IP3R1/GAPDH
Nav1.5/GAPDH

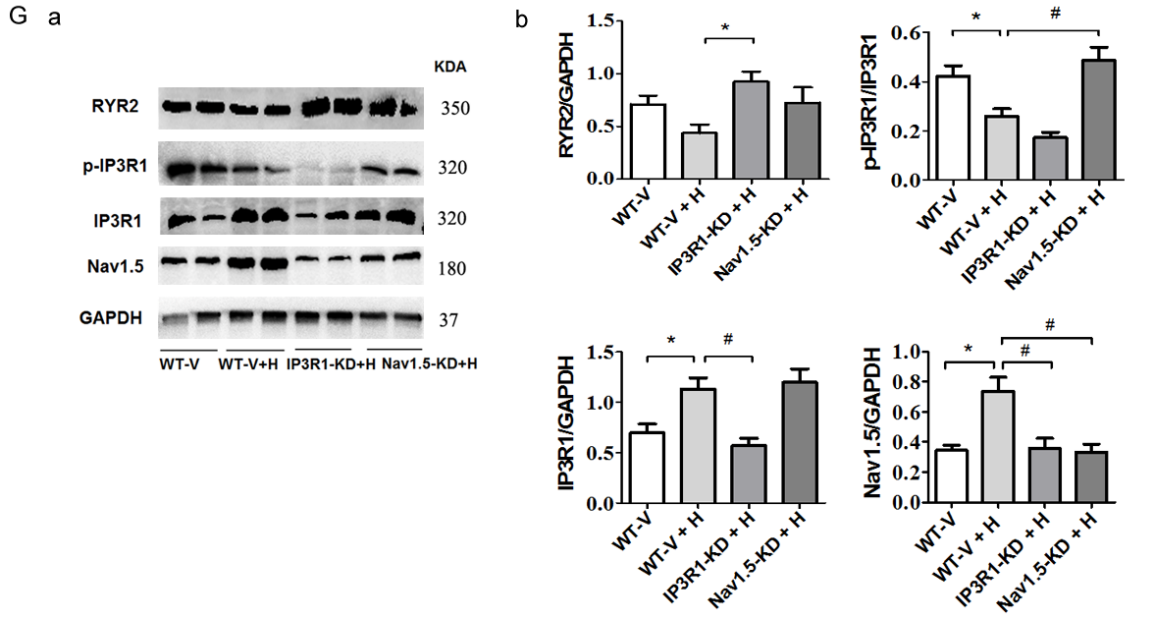

Figure 3. Hcy increases IP_3R1 and Nav1.5 expression at protein level, but it decreases the level of p-IP_3R1 and RyR2. Inhibition of Nav1.5 or IP_3R1 can alleviate the effect of Hcy *in vivo and in vitro experiments*, including increase in the levels of IP_3R1 and Nav1.5 level. WBs from 3 independent experiments (n = 3 total biological replicates per treatment; mean ± SEM) is plotted. (A) Representative WBs illustrating the detection of related proteins in lysates from MACs with different concentration of Hcy. (B) Western blot analysis to test the expression changes of associated proteins under Hcy stimulation with or without ELE or 2APB. (C, D) Western blot analysis to test the expression changes of related proteins in the lysates from MACs transfected with IP_3R1-shRNA or Nav1.5-shRNA and after exposure to Hcy stimulation for 48 h or not. (E) C57B6 mice at 1 week were injected with purified AAV9-GFP (vector), AAV9-Nav1.5-shRNA, or Ad-IP_3R1-shRNA via the caudal vein (termed WT-V, IP_3R1-KD and Nav1.5-KD mice). WT-V mice were fed a high-Hcy diet (IP_3R1-KD + H, Nav1.5-KD + H) at 4 weeks of age. (F, G) Representative WBs testing the change in levels of related proteins in MACs from WT-V mice, IP_3R1-KD and Nav1.5-KD mice fed a normal or high-Hcy diet. Error line indicates mean and standard deviation. Unpaired t-test was used for (A-D, F, G).

cess of Ca^{2+}-induced Ca^{2+} release (CICR) [9, 25, 28]. Moreover, excessive Na^+ and Ca^{2+} influx can cause early (EAD) and delayed (DAD) afterdepolarizations, and eventually induce APDs prolongation, which is known as a pathology of electrical remodeling [25]. We detected disorder of electrical activities in response to Hcy, including enhanced I_{NaL} and I_{CaL} levels, Ca^{2+} accumulation, and APDs prolongation. Then, we established cardiac-specific IP_3R1 or Nav1.5 knockdown model *in vivo and in vitro experiments*, and affirmed that the pro-arrhythmic effect of Hcy could be completely blunted in the above models. Interestingly, the effect of knocking down of IP_3R1 gene on the inhibition of APDs prolongation was greater than blocking Nav1.5 gene, which implied that the contribution of IP_3R1 in modulating the process of Ca^{2+} homeostasis was greater than that of Nav1.5. In addition, IP_3R1 and Nav1.5 co-localized in the nucleus of MACs, and the interaction was enhanced under Hcy stimulation. Interestingly, Hcy could decrease the co-localization between p-IP_3R1 and Nav1.5, which may be due to the IP_3R1 protein dephosphorylated after Hcy stimulation. Thus, above evidence confirmed that IP_3R1/Nav1.5 axis contributes to the process of Hcy-induced Na^+ and Ca^{2+} influx, and subsequently cause Ca^{2+} accumulation. We further investigate the IP_3R1 is how to regulate Nav1.5 activity as the basis of electrical remodeling under Hcy stimulation.

In vivo experiment, we observed the decreased Nav1.5 protein levels in the IP_3R1-KD model, but the expression levels of IP_3R1 was no apparent changes in the Nav1.5-KD model. Similarly, *in vitro experiment*, Nav1.5 expression was inhibited in the HH + 2APB groups, compared to the HH groups, even if the IP_3R1 protein level was not significantly altered in the HH + ELE groups. This finding suggested that Hcy initiates IP_3R1 up-regulation, and then modulates downstream protein, Nav1.5.

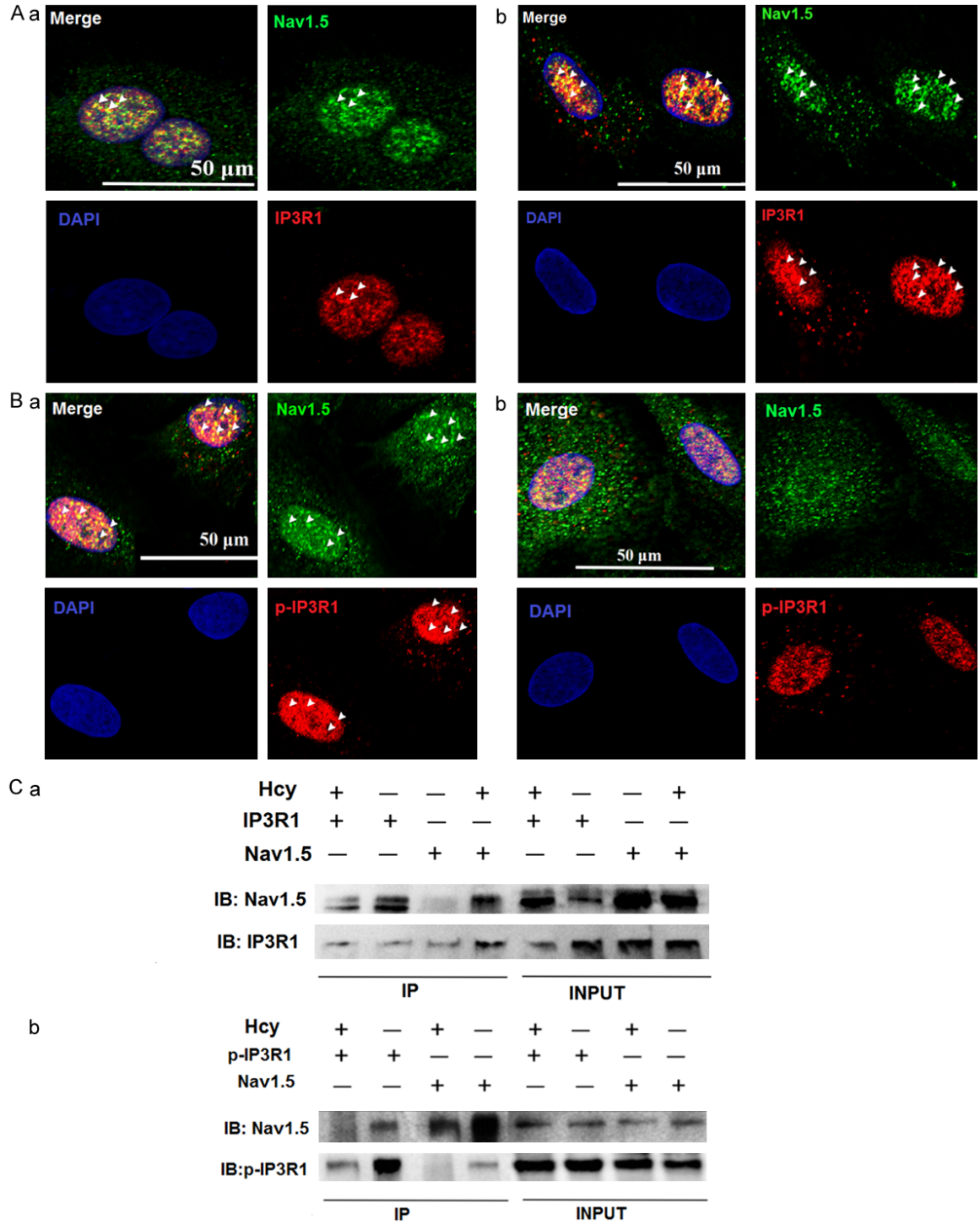

Figure 4. Hcy can increase the interaction between IP_3R1 and Nav1.5. However, Hcy decrease the co-localization of p-IP_3R1 (ser1756) and Nav1.5. (A) Cells were co-stained with antibodies against Nav1.5 (Alexa Fluor 488, green) and IP_3R1 or p-IP_3R1 (Alexa Flour 564, red). Arrows indicate co-localization. (a) Co-localization between IP_3R1 and Nav1.5 in the control groups; (b) Co-localization between IP_3R1 and Nav1.5 following Hcy treatment for 48 h. The interactions were higher than the control groups. (B) (a) Interaction between Nav1.5 and p-IP_3R1 in mammalian cells by co-IP; (b) Co-localization between p-IP_3R1 and Nav1.5 following Hcy treatment for 48 h. The interactions were lower than the control groups. (C) (a) Interaction of Nav1.5 and IP_3R1 in Hcy treated cells are stronger than in the control groups; (b) Hcy stimulation decreases the interaction of endogenous Nav1.5 and p-IP_3R1.

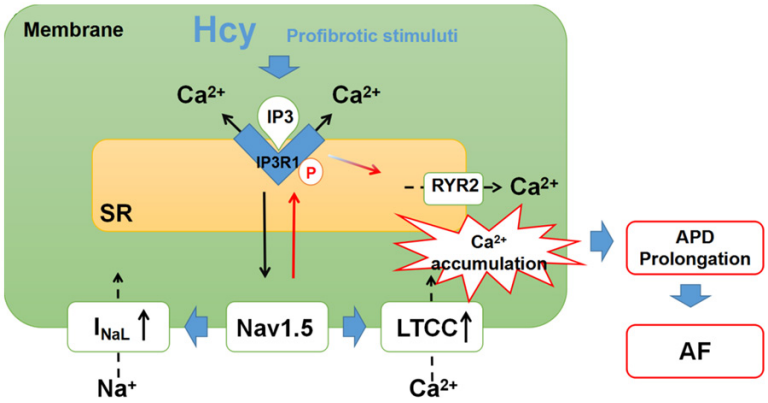

Figure 5. Hcy promotes IP_3R1 up-regulation, enhances Nav1.5 activity, and elevates I_{NaL} and I_{CaL} under Hcy stimulation, but Nav1.5 decreases the level of phosphorylated IP_3R1. This decreases the contribution of RyR2 to Ca^{2+} leakage from the SR, as a compensatory mechanism. Ca^{2+} influx leads to the APDs prolongation associated with AF pathology. The specific mechanisms of AF require further investigation.

Strikingly, the phosphorylated levels of IP_3R1 increased in the Nav1.5-KD + HH mice, which could be explained by the evidence that Nav1.5 can trigger the reversible dephosphorylation of IP_3R1. Early study also affirmed that IP_3R1 phosphorylation inhibited IP_3-dependent Ca^{2+} release [26]. Therefore, it both implies that a decreased p-IP_3R1 level aggravates IP_3-dependent Ca^{2+} release, which is consistent with the result of IP_3R1 protein in dephosphorylated state under stimulus. It is noteworthy that an external mechanism is involved in the process of IP_3R1-mediated electrical remodeling. RyR2, a channel for mediating excitation-contraction (E-C) coupling, is closely associated with the IP_3Rs family, and shares a high structural homology [26]. Although the expression of IP_3Rs in the myocardium is 50-fold lower than RyR2, IP_3Rs are primarily located in the atrial myocyte, compared with the RyR2 distribution in ventricle myocyte. In this study, the expression levels of RyR2 were decreased under Hcy stimulation because of a compensatory mechanism that maintains Ca^{2+} homeostasis in the atrium via the down-regulation of RyR2 [27-29]. This results further demonstrate that IP_3R1 plays an indispensable role in mediating Ca^{2+} signaling pathway in atrium.

Combined with the above evidence, we concludes that IP_3R1/Nav1.5 axis plays a critical role in modulating $[Ca^{2+}]_i$ homeostasis and subsequently promotes the electrical remodeling in the atrium under Hcy stimulation, which is regarded as a potential targeted-therapy for patients with atrial arrhythmias, especially for AF patients with hyperhomocysteinemia (**Figure 5**).

Acknowledgements

We are grateful to Dr. Juxiang Li for carefully reading and revising the manuscript. This work was supported by grants from the National Natural Science Foundation of China (8176020206 to J. Li), Jiangxi Natural Science Foundation (20152ACB20025 to J. Li) and the Science and Technology Support of Jiangxi Province (20151BB-G70166 to J. Li).

Disclosure of conflict of interest

None.

Address correspondence to: Dr. Juxiang Li, Department of Cardiovascular Medicine, The Second Affiliated Hospital of Nanchang University, Nanchang 330006, China. Tel: +86-13657092311; E-mail: ljx912@126.com

References

[1] Wu W, Liu J, Li A, Li J, Yang Y, Ye X and Zheng J. Effect of intensive blood pressure control on carotid morphology and hemodynamics in Chinese patients with hyperhomocysteinemia-type hypertension and high risk of stroke. Med Sci Monit 2019; 25: 5717-5726.

[2] Naji F, Suran D, Kanic V, Vokac D and Sabovic M. High homocysteine levels predict the recurrence of atrial fibrillation after successful electrical cardioversion. Int Heart J 2010; 51: 30-33.

[3] Iguchi M, Tezuka Y, Ogawa H, Hamatani Y, Takagi D, An Y, Unoki T, Ishii M, Masunaga N, Esato M, Tsuji H, Wada H, Hasegawa K, Abe M, Lip GYH and Akao M. Incidence and risk factors of stroke or systemic embolism in patients with atrial fibrillation and heart failure-The Fushimi AF Registry. Circ J 2018; 82: 1327-1335.

[4] Mueller KAL, Heinzmann D, Klingel K, Fallier-Becker P, Kumbrink J, Langer H, Schreieck J, Gramlich M, Gawaz M and Seizer P. Histopathological and immunological characteristics of tachycardia-induced cardiomyopathy. J Am Coll Cardiol 2017; 69: 2160-2172.

[5] Kolodziejczyk-Czepas J, Talar B, Nowak P, Olas B and Wachowicz B. Homocysteine and its thi-

olactone impair plasmin activity induced by urokinase or streptokinase in vitro. Int J Biol Macromol 2012; 50: 754-758.
[6] Yue ZJ, Xu PT, Jiao B, Chang H, Song Z, Xie MJ and Yu ZB. Nitric Oxide protects L-type calcium channel of cardiomyocyte during long-term isoproterenol stimulation in tail-suspended rats. Biomed Res Int 2015; 2015: 1-13.
[7] Doleschal B, Primessnig U, Wölkart G, Wolf S, Schernthaner M, Lichtenegger M, Glasnov TN, Kappe CO, Mayer B, Antoons G, Heinzel F, Poteser M and Groschner K. TRPC3 contributes to regulation of cardiac contractility and arrhythmogenesis by dynamic interaction with NCX1. Cardiovascular Res 2015; 106: 163-173.
[8] Liang X, Xie H, Zhu PH, Hu J, Zhao Q, Wang CS and Yang C. Enhanced activity of inositol-1,4,5-trisphosphate receptors in atrial myocytes of atrial fibrillation patients. Cardiology 2009; 114: 180-191.
[9] Cheng H and Wang SQ. Calcium signaling between sarcolemmal calcium channels and ryanodine receptors in heart cells. Front Biosci 2002; 7: 1867-1878.
[10] Yamamoto-Hino M, Sugiyama T, Hikichi K, Mattei MG, Hasegawa K, Sekine S, Sakurada K, Miyawaki A, Furuichi T and Hasegawa M. Cloning and characterization of human type 2 and type 3 inositol 1,4,5-trisphosphate receptors. Recept Channels 1994; 2: 9-22.
[11] Amroudie MN and Ataei F. Experimental and theoretical study of IBC domain from human IP3R2; molecular cloning, bacterial expression and protein purification. Int J Biol Macromol 2019; 124: 1321-1327.
[12] Yamada J, Ohkusa T, Nao T, Ueyama T, Yano M, Kobayashi S, Hamano K, Esato K and Matsuzaki M. Up-regulation of inositol 1,4,5 trisphosphate receptor expression in atrial tissue in patients with chronic atrial fibrillation. J Am Coll Cardiol 2001; 37: 1111-1119.
[13] Gambardella J, Trimarco B, Iaccarino G and Santulli G. New insights in cardiac calcium handling and excitation-contraction coupling. Adv Exp Med Biol 2018; 1067: 373-385.
[14] Li X, Zima AV, Sheikh F, Blatter LA and Chen J. Endothelin-1-induced arrhythmogenic Ca^{2+} signaling is abolished in atrial myocytes of inositol-1,4,5-trisphosphate(IP_3)-receptor type 2-deficient mice. Circ Res 2005; 96: 1274-1281.
[15] Paknejad N and Hite RK. Structural basis for the regulation of inositol trisphosphate receptors by Ca^{2+} and IP_3. Nat Struct Mol Biol 2018; 25: 660-668.
[16] Pezhouman A, Cao H, Fishbein MC, Belardinelli L, Weiss JN and Karagueuzian HS. Atrial fibrillation initiated by early afterdepolarization-mediated triggered activity during acute oxidative stress: efficacy of late sodium current blockade. J Heart Health 2018; 4: 1-17.
[17] Avula, UMR, Abrams J, Katchman A, Zakharov S, Mironov S, Bayne J, Roybal D, Gorti A, Yang L, Iyer V, Waase M, Saluja D, Ciaccio EJ, Garan H, Marks AR, Marx SO and Wan EY. Heterogeneity of the action potential duration is required for sustained atrial fibrillation. JCI Insight 2019; 4: 1-12.
[18] Yoo S, Aistrup G, Shiferaw Y, Ng J, Mohler PJ, Hund TJ, Waugh T, Browne S, Gussak G, Gilani M, Knight BP, Passman R, Goldberger JJ, Wasserstrom JA and Arora R. Oxidative stress creates a unique, CaMKII-mediated substrate for atrial fibrillation in heart failure. JCI Insight 2018; 3: 1-22.
[19] Mitchell KJ, De Clercq D, Stirn M, van Loon G and Schwarzwald CC. Plasma homocysteine concentrations in healthy horses and horses with atrial fibrillation. J Vet Cardiol 2018; 20: 276-284.
[20] Burashnikov A and Antzelevitch C. Role of late sodium channel current block in the management of atrial fibrillation. Cardiovasc Drugs Ther 2013; 27: 79-89.
[21] Go LO, Moschella MC, Watras J, Handa KK, Fyfe BS and Marks AR. Differential regulation of two types of intracellular calcium release channels during end-stage heart failure. J Clin Invest 1995; 95: 888-894.
[22] Yamada J, Ohkusa T, Nao T, Ueyama T, Yano M, Kobayashi S, Hamano K, Esato K and Matsuzaki M. Upregulation of inositol 1,4,5-trisphosphate receptor expression in atrial tissue in patients with chronic atrial fibrillation. J Cardiol 2002; 39: 57-58.
[23] Liang X, Xie H, Zhu PH, Hu J, Zhao Q, Wang CS and Yang C. Enhanced activity of inositol-1,4,5-trisphosphate receptors in atrial myocytes of atrial fibrillation patients. Cardiology 2009; 114: 180-191.
[24] Parekh AB. Regulation of CRAC channels by Ca2+-dependent inactivation. Cell Calcium 2017; 63: 20-23.
[25] Giorgi C, Marchi S, and Pinton P. The machineries, regulation and cellular functions of mitochondrial calcium. Nat Rev Mol Cell Biol 2018; 19: 713-730.
[26] Murthy KS and Zhou H. Selective phosphorylation of the IP3R-I in vivo by cGMP-dependent protein kinase in smooth muscle. Am J Physiol Gastrointest Liver Physiol 2003; 284: 221-230.
[27] Cheng H, Lederer WJ and Cannell MB. Calcium sparks: elementary events underlying excitation-contraction coupling in heart muscle. Science 1993; 262: 740-744.

[28] Ohkusa T, Ueyama T, Yamada J, Yano M, Fujumura Y, Esato K and Matsuzaki M. Alteration in cardiac sarcoplasmic reticulum Ca2+ regulatory protein in the atrial tissue of patients with chronic atrial fibrillation. J Am Coll Cardiol 1999; 34: 255-263.

[29] Yoo S, Aistrup G, Shiferaw Y, Ng J, Mohler PJ, Hund TJ, Waugh T, Browne S, Gussak G, Gilani M, Knight BP, Passman R, Goldberger JJ, Wasserstrom JA and Arora R. Oxidative stress creates a unique, CaMKII-mediated substrate for atrial fibrillation in heart failure. JCI Insight 2018; 3: 1-22.

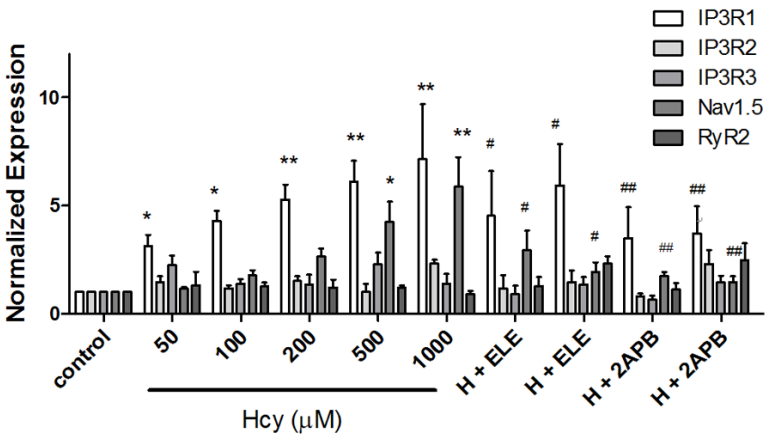

Figure S1. Hcy can increases the expression of IP_3R1 and Nav1.5, but not that of IP_3R2 or IP_3R3. Bar graph illustrating the different isoforms of IP_3Rs and RYR2 at the transcript level following Hcy stimulation in the presence of ELE, or 2APB. *P<0.05 and **P<0.01 vs control; #P<0.05, ##P<0.01 vs (1 mM) Hcy group. (n = 5). Unpaired t-test was applied for calculating data.

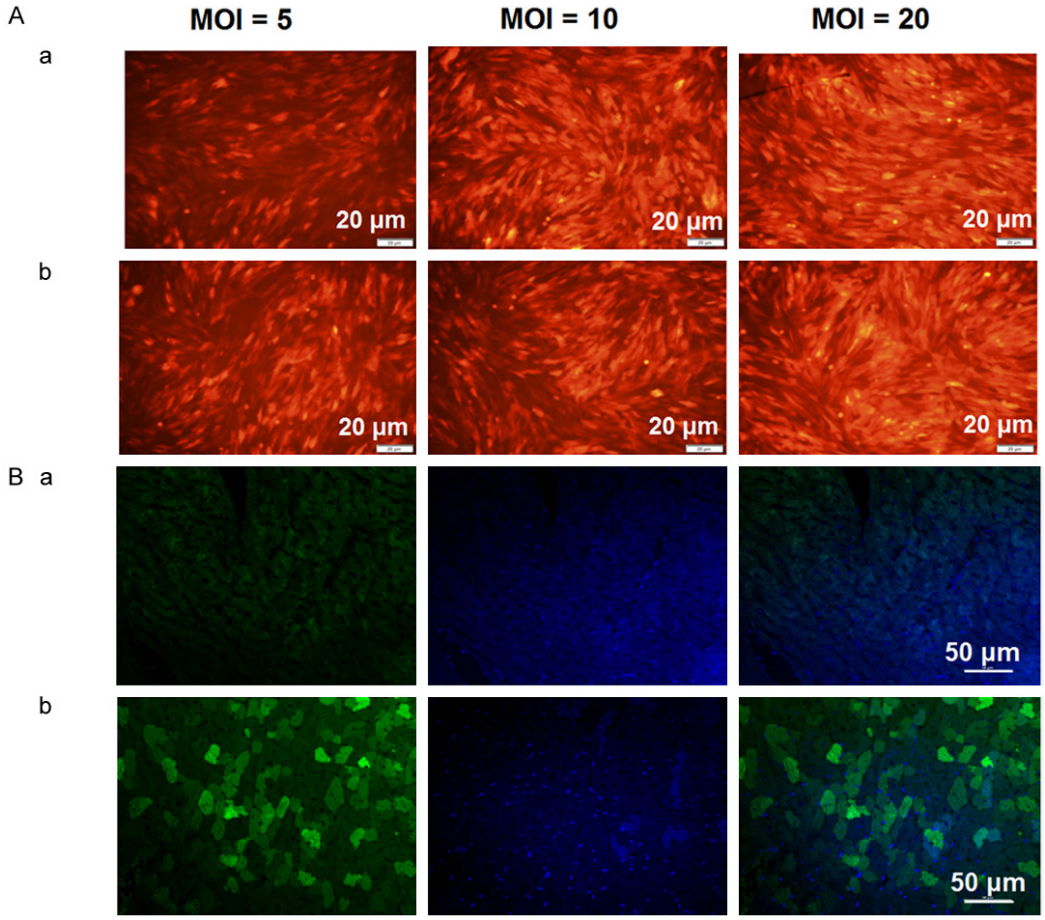

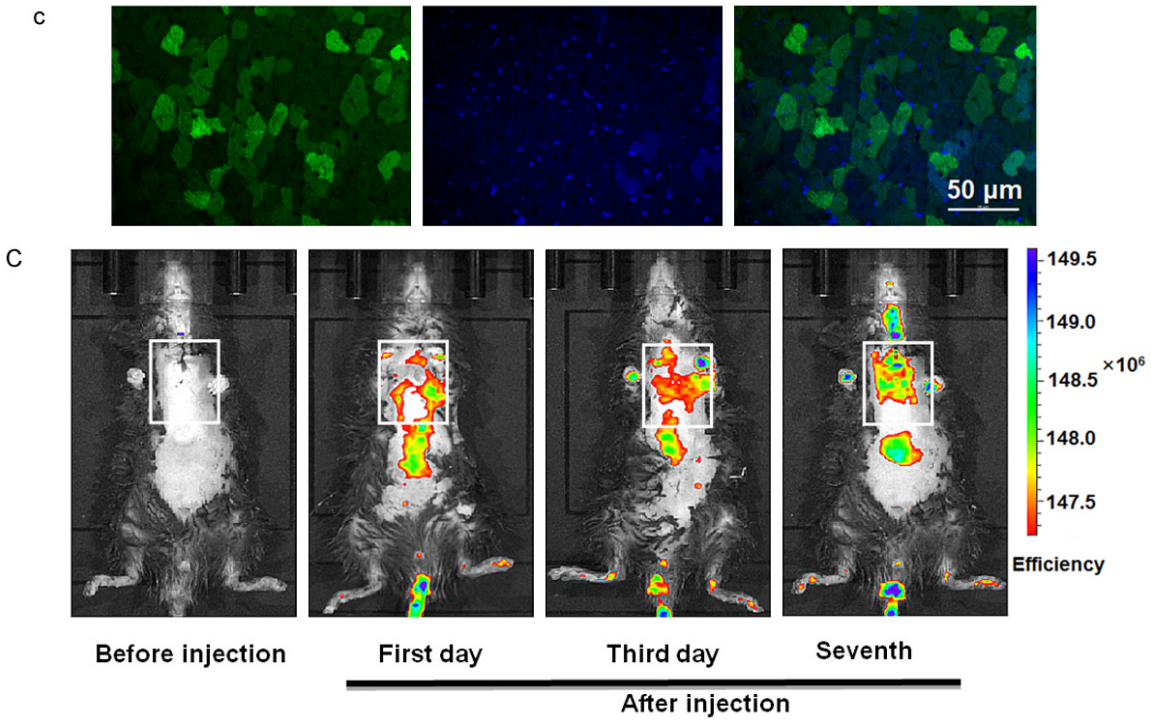

Figure S2. Successful knockdown model of IP_3R1 and Nav1.5 by lentiviral transferred siRNA *in vivo and in vitro*. (A) Cell morphology of MACs infected with AAV-9 imaged by fluorescence microscopy (A: a, IP_3R1-shRNA group; A: b, Nav1.5-shRNA group, MACs showed red fluorescence after AAV9 infection; MOI = 5, 10, 20, respectively; ×20). B: Cell morphologies of the atrial myocytes isolated from adult mice injected with AAV-9 detected by confocal fluorescence microscopy (B: a, WT-V group; B: b, IP_3R1-KD group, and B: c, Nav1.5-KD group). MACs showed green fluorescence following AAV9 infection; MOI = 100, respectively; ×20). (C) The transfection efficiency of AAV9-vectors on cardiac function from days 0-7 assessed by fluorescent microscopy.

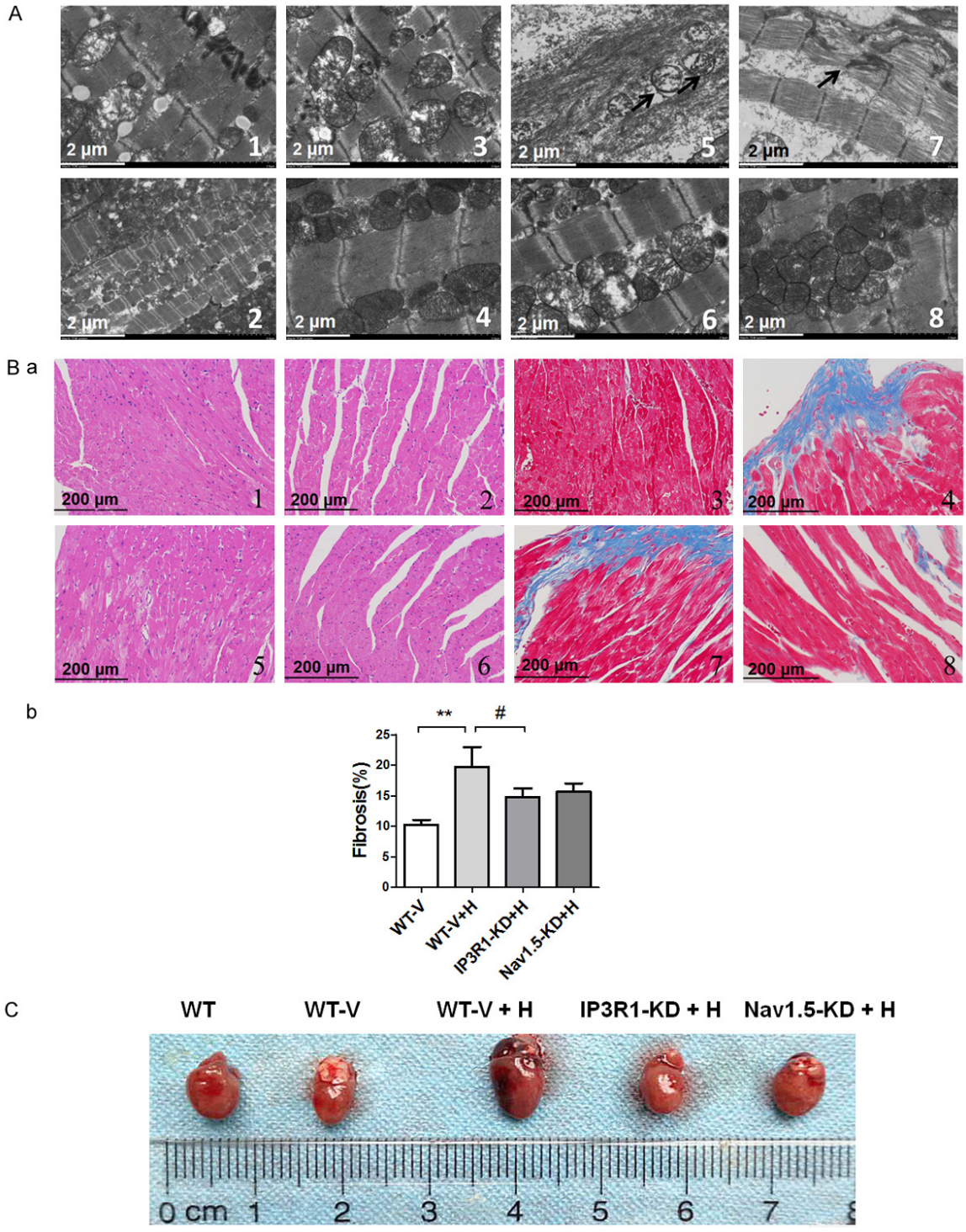

Figure S3. Hcy causes fibrosis and myofibrillation in atrial tissue. (A) Ultra-structure of atrial tissues examined via electron microscopy. (1, 5) WT mice fed with normal diet (WT); (2, 7) WT mice fed with high-Hcy diet (WT + H); (3, 6) IP_3R1-KD mice fed with high-Hcy diet (IP_3R1-KD + H); (4, 8) Nav1.5-KD mice fed a High-Hcy diet (Nav1.5-KD + H). Black arrows: rupturing of the fascicle, loose arrangements of both crude and fine filaments, hyperplasia, and disordered mitochondrial cristae. (B) (a1-a2, a5-a6) Photomicrograph of HE staining of MACs in WT-V (a1), WT-V + H (a2), IP_3R1-KD + H (a5), and Nav1.5-KD + H (a6). (a3-a4, a7-a8) Masson's trichrome staining of MACs in WT-V (a3), WT-V + H (a4), IP_3R1-KD + H (a7), and Nav1.5-KD + H (a8) (magnification ×200; scale bar = 200 μm; n = 4). (B) (b) Positive areas and their ratios to the total area of the fibers are shown. Multiple t-tests were performed. (C) Cardiac sizes across the different groups.